JOURNAL OF AIRCRAFT
Vol. 45, No. 4, July–August 2008

# Experimental Investigation on Modal Signature of Smart Spring/Helicopter Blade System

G. Coppotelli*
*Sapienza Università di Roma, 00184 Rome, Italy*
P. Marzocca†
*Clarkson University, Potsdam, New York 13699*
and
F. D. Ulker,‡ J. Campbell,§ and F. Nitzsche¶
*Carleton University, Ottawa, Ontario K1S 5B6, Canada*

DOI: 10.2514/1.35139

**To achieve efficient attenuation of noise and vibration characteristics within the helicopter environment, solid-state actuators are seen as one of the most promising smart technologies. The Smart Hybrid Active Rotor Control System project is expected to demonstrate the ability of smart structure systems, employing multiple active material actuators, sensors, and closed-loop controllers, to reduce simultaneously rotorcraft vibration and noise. Within this project, piezoceramic elements were used as actuators to vary the dry friction and the stiffness of the whole helicopter blade system. This active control concept, named Smart Spring, originated a prototype used to demonstrate the ability to attenuate vibrations. Before testing the Smart Hybrid Active Rotor Control System in operative conditions, the dynamic properties of the Smart Spring installed on a nonrotating helicopter blade are investigated. The effects of the Smart Spring actuator on the modal properties are studied through experimental activities carried out at Carleton University. Furthermore, the capability of the Smart Spring to change the dynamic behavior of the helicopter blade is demonstrated by analyzing the shifts in the modal parameters. Finally, a beam finite element model of the blade, with stiffness and mass properties tuned to the experimental structure, is presented.**

## I. Introduction

THE most important components of noise and vibration produced in helicopters originate from the main rotor due to the unsteady aerodynamics that characterize high-speed forward, maneuvering, and descent flight regimes. Low-frequency vibration is mostly generated by dynamic stall in the reverse-flow region at high forward speeds. High-frequency acoustic noise is produced mainly in maneuvering and descent flight regimes when the rotor blades interact with the vortices shed by the tip of preceding blades, resulting in the phenomenon known as blade vortex interaction (BVI). This interaction leads to an impulsive change in the blade loading, which generates a pressure perturbation in the flowfield above and below the rotor disk. The perturbation then propagates as a pressure wave below the rotor disk and reaches the ground in the form of a strong slapping noise. Recent experiments in Europe with the individual blade control (IBC) approach indicated that only marginal reduction of both noise and vibration can be obtained simultaneously, although significant reductions of each are possible individually [1]. These findings were confirmed by recent works [2–5], where active control experiments and numerical investigations were performed to measure noise and vibration. In those activities, it was noted by the authors that introducing control inputs that reduce vibration has the counterpart of increasing the noise and vice versa. The explanation for this fact would be the apparent conflict of the philosophy used in the control objectives, that is, "smoothing" the flight of the blade to achieve vibration reduction, while simultaneously avoiding intersection with the path of the impinging vortices to achieve noise attenuation.

Carleton University coordinates the Smart Hybrid Active Rotor Control System (SHARCS) project, providing the various designs of the active control subsystems and developing the related software. The project is cosponsored in Canada by the Natural Sciences and Engineering Research Council and the Ontario Center of Excellence Materials Manufacturing of Ontario. In addition, Sensor Technology, Ltd., Canada, provides smart sensors and actuators, and Agusta S.p.A. of Italy will supply a small-scale rotor driving mechanism, scaled blade hardware, a slip ring rotor data collection system, and noise and vibration suppression requirements of a typical helicopter rotor. Other international partners of the project include the Polytechnic of Milan, University of Rome "La Sapienza," the University of Rome "Tre" (Italy), the National Technical University of Athens (Greece), and Clarkson University (United States). The final aim of the SHARCS project is to develop a "hybrid" control concept consisting of separate flow and structural control subsystems. An idealization of such an approach is seen in Fig. 1. This approach would have potential to reduce noise and vibration simultaneously because the problems of vibration and noise are handled by two completely independent feedback subsystems. As described in Fig. 1, the Smart Spring actuator [6] placed at the blade root would attenuate the vibration, whereas the active shape control at the tip of the blade would reduce noise. The Smart Spring is an active vibration control concept that uses piezoceramic actuators to preferentially vary dry friction and stiffness of a structure. This device, if located at the blade root, could adaptively vary the dynamic stiffness of the blade to change its flexural characteristics, thus allowing control of the aeroelastic response of the entire blade. A real-time controller identifies the

Presented as Paper 2035 at the 47 AIAA/ASME/ASCE/AHS/ASC, Structures, Structural Dynamics, and Materials Conference, Newport, RI, 1–4 May 2006; received 15 October 2007; revision received 21 March 2008; accepted for publication 21 March 2008. 

*Assistant Professor, Dipartimento di Ingegneria Aerospaziale e Astronautica, Via Eudossiana, 16. AIAA Senior Member.

†Assistant Professor, Department of Mechanical and Aeronautical Engineering, The Wallace H. Coulter School of Engineering, CAMP 234. AIAA Member.

‡Ph.D. Student, Department of Mechanical and Aerospace Engineering.

§Undergraduate Student, Department of Mechanical and Aerospace Engineering.

¶Professor, Department of Mechanical and Aerospace Engineering. AIAA Senior Member.

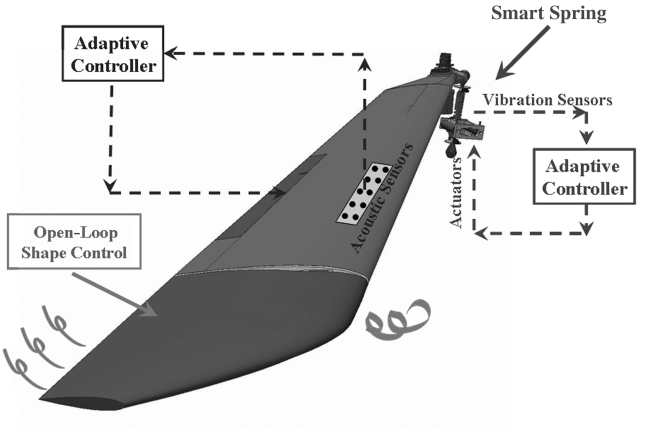


**Fig. 1 Hybrid control concept.**

variations in the structural dynamics caused by unsteady aerodynamic environment and attempts to maximize the performance [7]. Simulations and laboratory tests have already verified the ability of the Smart Spring to adaptively vary the structural impedance properties, suppressing low-frequency torsional aeroelastic response of a fixed wing to buffet loads [7]. As an addition to the Smart Spring, a suitably actuated trailing-edge flap could perform flow control by alleviating the negative effects of dynamic stall on the retreating side of the blade. This would reduce the vibration excitation loads at the origin of the phenomena [8]. In [8], it was shown that the required size of such a flap is relatively small, facilitating its integration within the blade, with the request of very small actuator loads. Finally, it has been demonstrated in separate studies that optimization of the blade anhedral tip angle can alleviate BVI at a fixed rotor attitude, by displacing the trajectory of the vortices that are shed at the tip of the blade [9]. Therefore, the Smart Spring flap system could be used as an adaptive mechanism capable of changing the aerodynamic characteristics of the flow. This could reduce noise under specific flight conditions.

In this paper, the results achieved during the first experimental activities devoted to characterize the Smart Spring device are presented. Because no previous experimental data were available, the test campaign started from the very beginning. Therefore, the influence of the Smart Spring device on the overall dynamic behavior of the rotor blade was initially investigated through an experimental modal survey. Thus, the main objective of this part of activities was to quantify the effects on the modal properties of different operating conditions of a prototype version of the Smart Spring device attached to the push rod of a full-scale Bell's helicopter blade. Such experimental investigation was of great importance for the SHARCS project because it cleared all the consequent other activities. By proving that the Smart Spring device was capable of affecting the modal properties of the helicopter blade, it could be possible to control its dynamic behavior to satisfy noise or vibration constraints by a suitable control law. The paper is organized as follows: in Sec. II, some insights on the Smart Spring device as a hybrid control actuator mechanism as used within the SHARCS project is presented; in Sec. III, the dynamic identification of the Smart Spring system through an experimental campaign performed at Carleton University is provided. An assessment of the finite element model developed for this blade is also included in Sec. IV of the paper. Finally, concluding remarks are reported in Sec. V.

## II. Feasibility Studies on the Smart Spring Device Mechanism

Most of the current active vibration control research activities focus on actively altering the time-varying aerodynamic loads on the blade to suppress vibration [5,7,8,10]. However, successful implementation of these approaches has been hindered by electromechanical limitations of smart material actuators by factors such as small stroke length [2,4,11]. Within the SHARCS program,

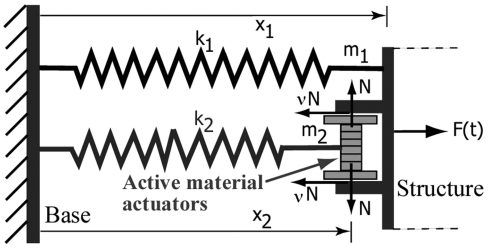


**Fig. 2 Smart Spring concept.**

an impedance control device is designed to adaptively alter the stiffness, damping, and effective mass of the blade to control the structural response. Such actuators could be operated by passive and active components, and, for this reason, it could be defined as a hybrid control actuator mechanism. One example of such a mechanism is shown in the conceptual drawing in Fig. 2. The system is optimized to exploit the large stiffness and bandwidth of piezoelectric materials to perform an indirect-active vibration suppression of axial loads. The device only requires the actuators to produce microdisplacement to generate relatively high actuation forces. The stacked piezoelectric actuators are able to achieve sufficient forces with less than 100 V peak-to-peak. The feasibility of this type of system is enhanced due to the use of relatively low driving voltages. In Fig. 2, the primary load-carrying spring system, whose $k_1$ and $m_1$ are the equivalent stiffness and mass, respectively, is attached to a vibrating structure to which an external force $F(t)$ is applied. The Smart Spring has a built-in sleeve consisting of a secondary spring $k_2$, a mass $m_2$, and the stacked piezoelectric actuator. When the actuator is OFF, primary and sleeve systems do not interact. Therefore, the response is determined by the single primary mass-spring system composed by the primary load-carrying spring and the actual structure. When the actuator is ON, a normal force $N(t)$ is generated and the secondary mass-spring system is engaged. With a sufficiently large resultant friction force $\nu N(t)$, the primary load-carrying spring, sleeve, and the structure become fully coupled. By varying the amount of voltage given to a piezoelectric actuator, the dynamic friction force can be regulated such that the stiffness, damping, and mass of the system can be continuously controlled.

## III. Dynamic Identification of the Smart Spring/ Helicopter Blade System

The sensitivities of the combined blade–Smart Spring actuator modal properties to different operating conditions are studied through experimental investigations carried out at Carleton University. The results presented in this work represent a final assessment of the preliminary activity already reported in [12]. The

**a) Experimental setup** **b) Detailed view of the excitation system**

**Fig. 3 Smart Spring/helicopter blade system.**

**Table 1 Measured voltage levels and corresponding force values**

| Working condition | Voltage level, V | Force, KN |
|---|---|---|
| OFF | 0.00 | 0.00 |
| ON | 0.05 | 0.21 |
| MEDIUM | 1.00 | 4.13 |
| HIGH | 2.00 | 8.26 |

system is composed of a Bell's helicopter blade (5.1 m span, 0.275 m chord, and a mass of 29.18 kg) and a prototype of the Smart Spring system which controls the stiffness and damping of the pitch link. The blade is hinged at the root and is suspended with a lumped spring support ($k = 463$ N/m) placed at about a three-quarter span from the root, as depicted in Fig. 3a. The different working conditions of the Smart Spring include the open-loop configurations OFF (smart spring disengaged), ON (smart spring engaged, i.e., low voltage), and two selected values of the normal actuator force (MEDIUM and HIGH voltages). Because the actuator is statically set to these values, that is, no feedback control is considered in the present study, only the feeding voltage levels are needed to univocally characterize the electrical parameters for each working condition. These are reported in Table 1, where the corresponding magnitudes of the actuator forces are also displayed. The modal survey has been carried out by exciting the system with a white noise disturbance applied at the trailing edge of the tip section of the blade using a vibration exciter from Bruel & Kjaer (Type 4808), as shown in Fig. 3b. The frequency response functions (FRFs) corresponding to 42 vertical accelerations, whose locations are sketched in Fig. 4, have been estimated in a frequency range of 0–128 Hz (using 4096 spectral lines, with 20

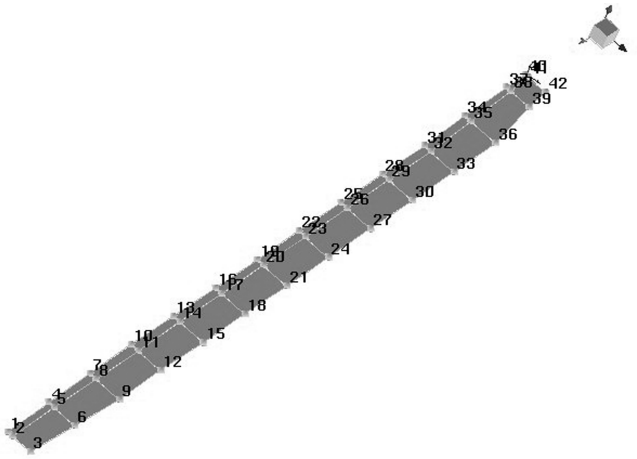

**Fig. 4 Schematic representation of the location of the experimental degrees of freedom.**

averages) by means of 6 PCB Piezoelectronics roving accelerometers (Type 352C22). The modal parameters, that is, natural frequencies $f_n$, damping ratios $\zeta_n$, and mode shapes, were estimated using the pole-residue approach by PolyMAX (Polyreference Modal Analysis Extended) [13]. This is a frequency domain based algorithm, provided by LMS International NV, especially suited for damped structures and larger bandwidths. PolyMAX is a polyreference version of the LSCF (least-square complex exponential in frequency domain) method [14], and uses a right matrix-fraction model [13,15]. The estimate procedure started

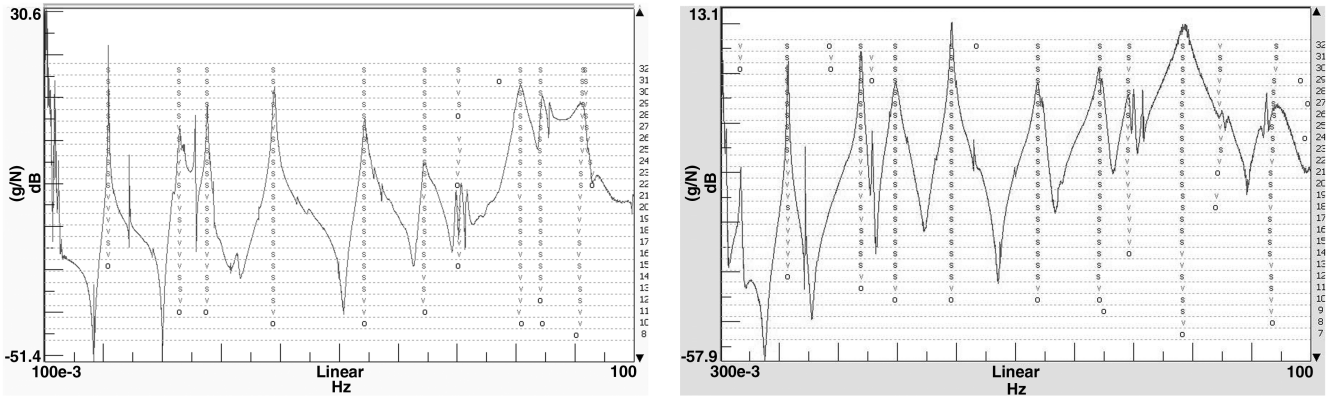


**a) Smart spring OFF** **b) Smart spring ON**

**Fig. 5 Identification of the poles of Smart Spring/blade system with PolyMAX.**

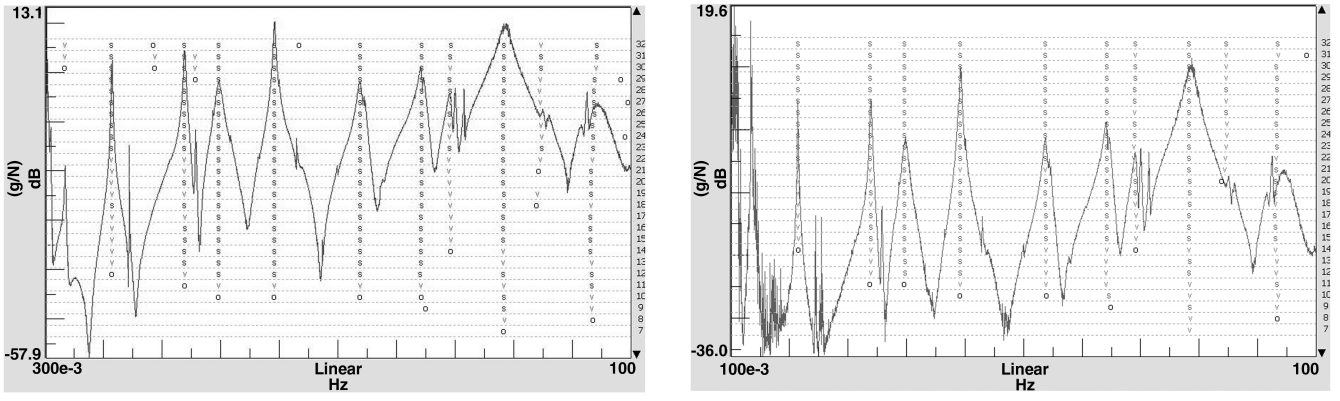


**a) Smart spring LOW** **b) Smart spring HIGH**

**Fig. 6 Identification of the poles of Smart Spring/blade system with PolyMAX.**

**Table 2 Mode type, natural frequencies, and damping ratios with Smart Spring OFF**

| Mode no. | Mode type[a] | $f_n$, Hz | $\zeta_n$, % |
|---|---|---|---|
| 1 | 1 F | N.A. | N.A. |
| 2 | 2 F | N.A. | N.A. |
| 3 | 3 F | 10.9262 | 0.16 |
| 4 | 3 F + 1 T | 22.8054 | 1.06 |
| 5 | 1 T | 27.6261 | 0.48 |
| 6 | 4 F | 38.9327 | 0.39 |
| 7 | 5 F | 54.3130 | 0.52 |
| 8 | 2 T | 90.8893 | 0.89 |

[a]F = flapwise bending, T = torsion

with the evaluation of the so-called stabilization diagrams, reported in Figs. 5 and 6 for the different actuation levels. The reference system is represented by the helicopter blade with the Smart Spring device in the OFF working condition. In each diagram, the poles identified by the estimating algorithm are displayed for each of the assumed number of modes of the system represented as different horizontal lines. Physical poles will always appear as, practically, independent of the assumed number of poles. In contrast, computational poles, modeling the noise on the data, are strongly dependent on the number of the assumed poles. Hence, the stabilization diagram not only gives a strong indication of the number of present poles, it also helps selecting the "best" estimate for the physical poles. Therefore, the accuracy of the estimate of the modal parameters depends on the frequency resolution adopted for the modal survey. Nevertheless, the procedure is not error free itself, because the poles are selected by the analyst. This selection is user dependent and it is based on the analyst's skill and experience. Also, the accuracy depends on how the vibrating structure is satisfying the main hypothesis of the linear system. Unfortunately, these two last sources of inaccuracy could not be quantified with numbers because the true model is, obviously, not known. Furthermore, the accuracy of the sensors and their placements (location and measurement directions) should be properly considered during data analysis. The "vertical" acceleration was the only data necessary for the identification procedure. This was provided by the accelerometers and the acquisition card. The adopted transducers are characterized by an almost unitary transfer function in the 10–10,000 Hz frequency band with an error due to the cross sensitivity to transverse acceleration, which could be neglected with respect to the others. The identified modal parameters for the reference system are reported in Table 2, where the mode types, natural frequencies, and damping ratios are shown. In addition, selected flapwise bending and torsional mode shapes are displayed in Figs. 7 and 8, respectively. The modal signature of the system did not capture the low-frequency modes, for example, the first and the second mode, because the first identified mode shape was the third out-of-plane bending mode. This is due to the low signal-to-noise ratio induced by the unavoidable moving parts of the whole system and to the low sensitivities, for frequencies as low as a few hertz, typical of the considered accelerometers. It is worth noticing that some additional structural poles were identified from the stabilization diagram in the 60–90 Hz range, but, because they most likely correspond to a prevalent in-plane bending coupling, they have not been considered in the identification process. The capability of the Smart Spring to change the dynamic behavior of the whole helicopter blade system is investigated through the analysis of the modal parameters achieved for the three actuation levels (ON, MEDIUM, and HIGH). Natural frequencies and damping ratios for the selected systems in the various working conditions are presented in Tables 3 and 4, respectively. Again, the accuracy of these estimates could be related to the frequency resolution as for the reference case. Although the changes in the natural frequencies and damping ratios corresponding to the flapwise bending modes are practically negligible, the corresponding shifts in the torsional eigenproperties are noticeably larger. The natural frequencies of the first and second torsional modes increase by almost 7.8 and 2.5%, respectively, as reported in Fig. 9, mostly due to the additional stiffness introduced by the Smart Spring device. On the other hand, the increase in the damping ratios for the first and second torsional modes, as compared with the reference case, are found to be greater than 250 and 130%, respectively, and depending on the operative condition, see Fig. 10. From these results, the effects of the Smart Spring actuator on the whole system could be outlined. From the experimental investigations, it appears that the Smart Spring device

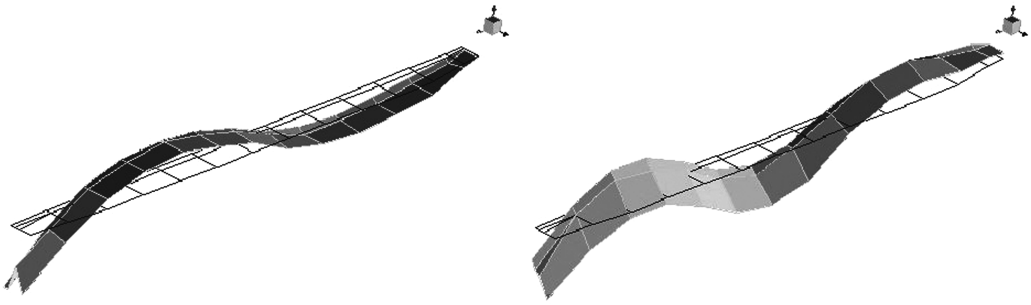

**a) Mode # 3 - $f_n$ = 10.9262 Hz** **b) Mode # 4 - $f_n$ = 22.8054 Hz**

**Fig. 7 Identified flapwise bending mode shapes with Smart Spring OFF.**

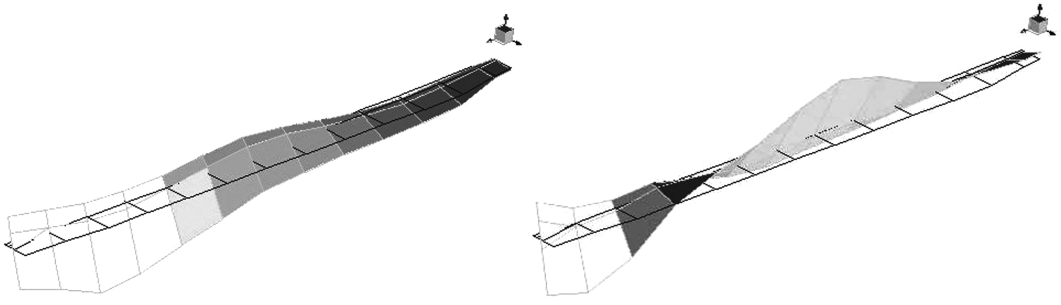

**a) Mode # 5 - $f_n$ = 27.6261 Hz** **b) Mode # 8 - $f_n$ = 90.8893 Hz**

**Fig. 8 Identified torsion mode shapes with Smart Spring OFF.**

**Table 3 Natural frequencies with engaged Smart Spring**

| Mode no. | Mode type | $f_n$, Hz, ON | $f_n$, Hz, MEDIUM | $f_n$, Hz, HIGH |
|---|---|---|---|---|
| 3 | 3 F | 11.525 | 11.526 | 11.532 |
| 4 | 3 F + 1 T | 23.926 | 23.926 | 23.932 |
| 5 | 1 T | 29.804 | 29.791 | 29.791 |
| 6 | 4 F | 39.255 | 39.254 | 39.239 |
| 7 | 5 F | 53.931 | 53.908 | 53.847 |
| 8 | 2 T | 93.197 | 93.217 | 93.468 |

**Table 4 Damping ratios with engaged Smart Spring**

| Mode no. | Mode type | $\zeta_n$, %, ON | $\zeta_n$, %, MEDIUM | $\zeta_n$, %, HIGH |
|---|---|---|---|---|
| 3 | 3 F | 0.429 | 0.449 | 0.424 |
| 4 | 3 F + 1 T | 0.576 | 0.610 | 0.546 |
| 5 | 1 T | 1.757 | 1.720 | 1.741 |
| 6 | 4 F | 0.434 | 0.438 | 0.440 |
| 7 | 5 F | 0.884 | 0.891 | 0.895 |
| 8 | 2 T | 2.134 | 2.313 | 2.705 |

introduces an (equivalent) additional torsional stiffness, as detected from the increase in the natural frequencies corresponding to the torsional modes. Moreover, this additional stiffness marginally depends on the actuation level for the first torsional mode, whereas it has some effects on the second torsional mode, as reported in Fig. 9. It is also reported that the Smart Spring device is capable of subtracting a considerable amount of dynamic energy from the system, especially in the pitch motion, as emphasized by the remarkable increase of the damping ratios associated with both of the identified torsional modes, see Fig. 10. As concerns the damping mechanism, it appears that the actuation level produces significant changes in the damping ratio associated with the second torsional mode, having no practical influence on the first one. From this point of view, a possible adaptive use of the Smart Spring system could be foreseen. Assuming the main contribution to the vibration of the blade is due to the pitch motion, it could be possible to control the vibration of the blade by adaptively changing the actuation level of the Smart Spring. The exploitation of the adaptive nature of the Smart Spring as a control device is outside the scope of this paper. The authors will present the results pertinent to the adaptive control strategies using the Smart Spring device as soon as the experimental data are available. The control authority in a 0.05–2.00 V range is capable of introducing an equivalent damping ratio that is a function of the actuation level and the operating frequency, as depicted in Fig. 11, where the damping ratio as a function of the frequency is plotted for each of the considered actuation levels. The changes in the dynamic response of the blade system due to the presence of the Smart Spring is also evident from the comparison between the driving point FRFs, evaluated in the OFF/ON Smart Spring operating condition. In Fig. 12, the system dynamic behavior, evaluated in the neighborhood of the first torsional frequency, has been highlighted. The peaks of resonance move to higher frequencies, from the reference to the ON condition value, and the resonant region is sensibly wider. Also, a reduction of the amplitude of the peak value, of about 10 dB on average, is clearly visible. This demonstrates the higher sensitivity to the different Smart Spring operating conditions of the damping mechanism associated with the actuator dynamics. This is an interesting finding of this experimental investigation because it represents, at least for the considered experimental setup, evidence of the effectiveness of the Smart Spring actuator in altering

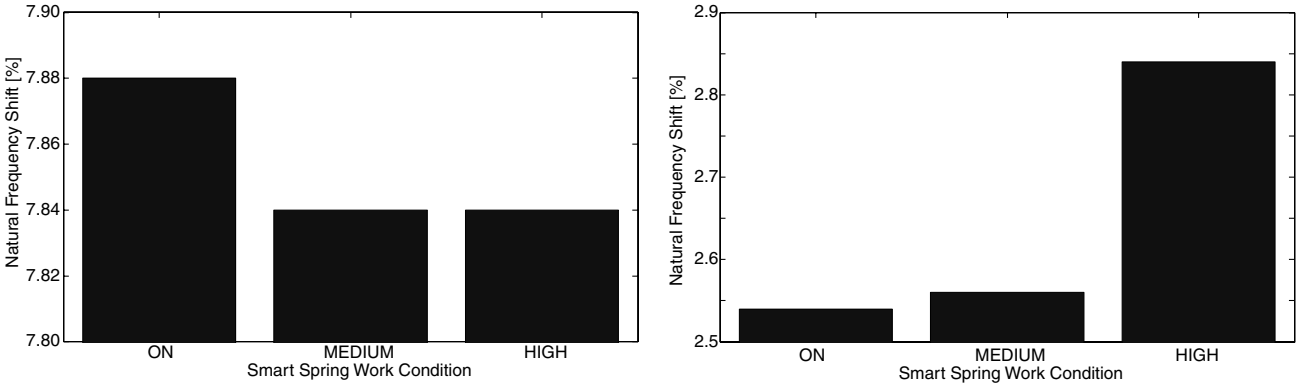


**a) Natural frequency sensitivity of the first torsional mode to Smart Spring operating conditions**

**b) Natural frequency sensitivity of the second torsional mode to Smart Spring operating conditions**

**Fig. 9 Natural frequency sensitivities to different Smart Spring operating conditions.**

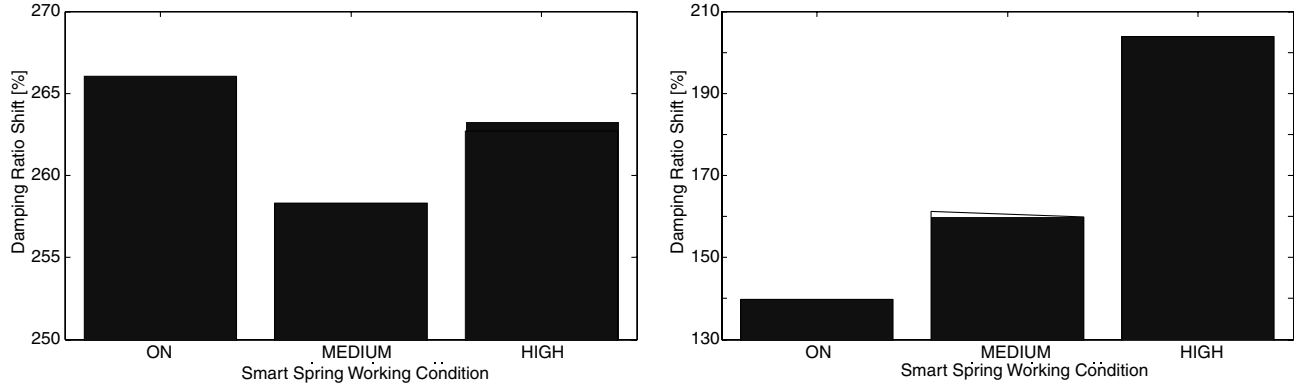


**a) Damping ratio sensitivity of the first torsional mode to Smart Spring operating conditions**

**b) Damping ratio sensitivity of the second torsional mode to Smart Spring operating conditions**

**Fig. 10 Damping ratio sensitivities to different Smart Spring operating conditions.**

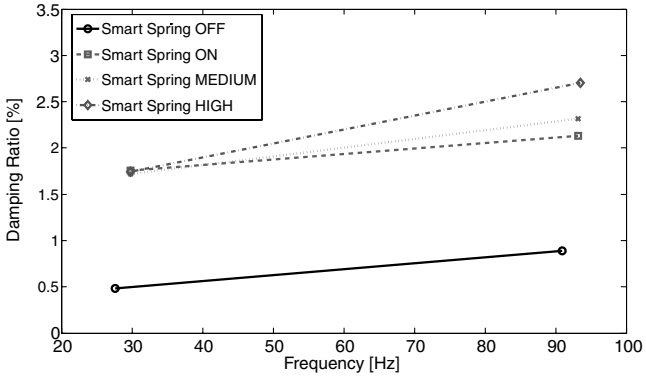


**Fig. 11 Damping ratio vs frequency for different Smart Spring working conditions.**

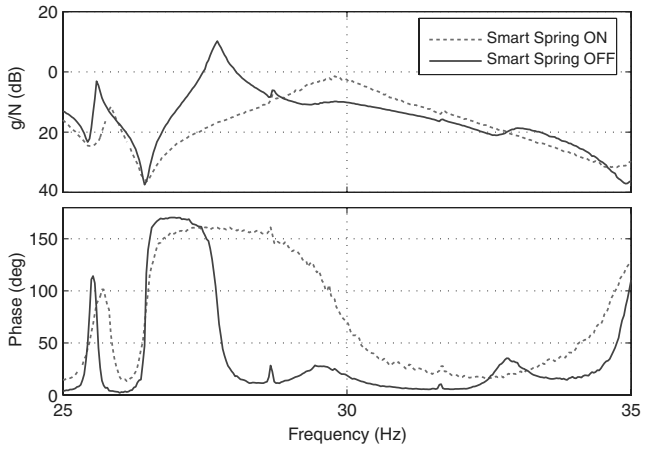


**Fig. 12 FRF comparisons for Smart Spring working conditions.**

the dynamics of the helicopter blade. Also, these preliminary results justify further experimental investigations aimed at verifying the actual control capabilities. A test campaign performed on a small-scale rotating blade is already planned in the near future.

## IV. Helicopter Blade Finite Element Model Assessment

In the following subsections, some ongoing numerical activities addressed to the development of a finite element model of the Smart Spring/helicopter blade system are presented. First, the stiffness properties, representative of the blade under investigation, gained by static tests [16], will be presented. Then, as a preliminary result, the correlation between the experimental and numerical modal model will be outlined in the last subsection.

### A. Geometrical and Structural Properties

Static analyses were performed to obtain the structural properties of the blade for each spanwise location considered in the finite element model. Because a beam element has been chosen to describe the dynamic behavior of the blade, the shear center chordwise position, the out-of-plane bending stiffness, and the torsional stiffness have been estimated as described in [16]. The obtained averaged values and some geometrical properties of the blade are given as follows: span 5.1 m, chord 0.275 m, thickness 0.047 m, mass 29.18 Kg, linear density 5.72 kg/m, out-of-plane bending stiffness (product of the equivalent Young modulus by the moment of inertia) $4.5 \times 10^3\ \mathrm{N \cdot m^2}$, torsional stiffness (product of the equivalent shear modulus by the torsional inertia) $4.66 \times 10^3\ \mathrm{N \cdot m^2}$. From the analysis of both the chordwise position of the shear center and the torsional stiffness, as a function of the different spanwise experimental locations, a small structural damage has been identified at approximately 40% of the blade span. This is illustrated in Figs. 13 and 14a, respectively. Corresponding to this section, the chordwise position of the shear center moves toward the trailing edge, whereas the torsional stiffness exhibits an evident loss of its value. In addition,

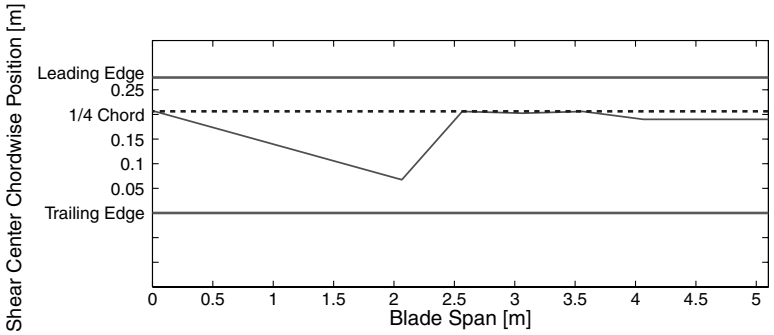


**Fig. 13 Identified shear center positions over the blade span (solid line = shear center, dotted line = quarter chord).**

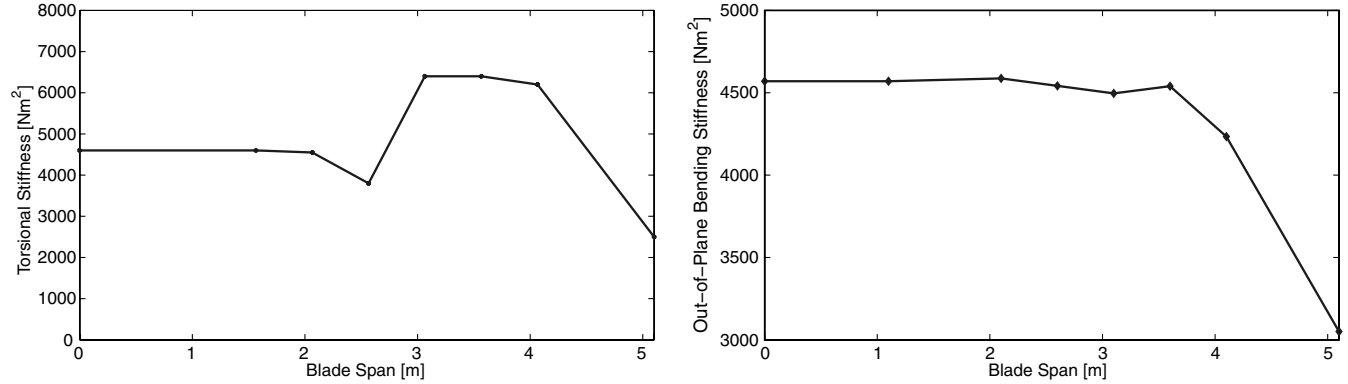


**a) Spanwise blade torsional distribution** **b) Spanwise blade out-of-plane stiffness distribution**

**Fig. 14 Estimate of the structural properties of helicopter blade from static tests.**

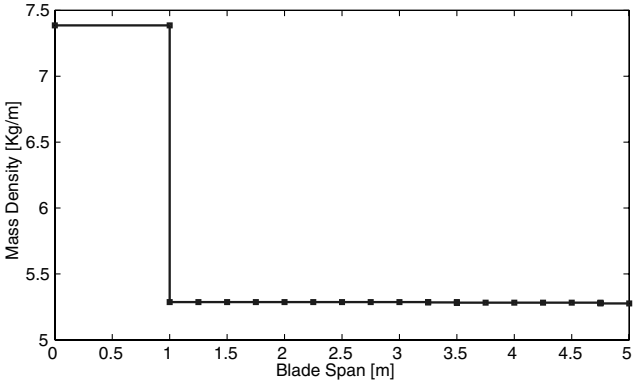


**Fig. 15 Assumed mass distribution over the blade span.**

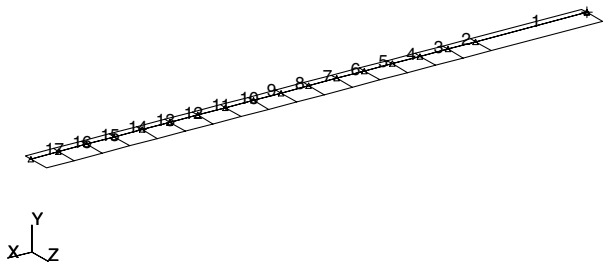


**Fig. 16 Blade finite element model.**

as reported in Fig. 14b, no particular trends for the out-of-plane bending stiffness are identified. Finally, the equivalent mass distribution used in the finite element (FE) model is reported in Fig. 15. This distribution has the property to keep the center of gravity of the blade in the same experimental position together with the total mass, as reported earlier in this paragraph.

### B. Correlation Between the Numerical/Experimental Dynamic Models

The finite element model of the blade structure is formed by 17 beam elements distributed over the blade span, as reported Fig. 16, defined over 18 grid points for a total of 54 degrees of freedom, that is, each grid is characterized by the out-of-plane deflection and bending rotation plus the pitch rotation. This blade "beam" model uses the previously identified structural properties. The stiffness related properties were directly considered when defining the beam finite element, whereas the inertial properties were included in the finite element model via elemental mass matrices defined for each grid. The presence of the Smart Spring in the pitch link has been modeled by a lumped torsional stiffness located at the blade root with the elastic constant tuned to the actual one, so that the differences between the numerical natural frequencies and the corresponding experimental ones were minimized. Moreover, the same finite element modeling has been adopted to consider the spring support positioned at three-quarters of the blade span, Fig. 3a. The resulting natural frequencies are reported in Table 5. Considering the errors in the estimate in the natural frequencies, fourth column of Table 5, it could be stated that the third out-of-plane bending and the first torsional modes are well identified by this "stick" FE model. In addition, a very high correlation between the mode shapes was found. As an example, the Modal Assurance Criterion value evaluated for modes 3 and 4 are as high as 97 and 91%, respectively, as one would expect by a visual inspection of the numerical modes, reported in Fig. 17, and the corresponding experimental ones, depicted in Fig. 7. Future developments will consider a 3-D dynamic model to take into consideration the flap-lag-pitch coupled dynamic behavior required for an accurate numerical analysis aimed to evaluate the effectiveness of the Smart Spring system for the rotor vibration reduction.

**Table 5 Numerical mode type, natural frequency, and relative error with respect to the experimental reference system**

| Mode no. | Mode type[a] | $f_n$ (Hz) | $\varepsilon$ (%) |
|---|---|---|---|
| 1 | 1 F | 1.0387 | N.A. |
| 2 | 2 F | 3.9316 | N.A. |
| 3 | 3 F | 11.1535 | −2.08 |
| 4 | 3 F + 1 T | 22.1684 | 2.79 |
| 5 | 1 T | 27.6072 | 0.07 |
| 6 | 4 F | 37.4942 | 3.69 |
| 7 | 5 F | 57.1931 | 5.30 |
| 8 | 2 T | 81.0276 | 10.85 |

[a]F = flapwise bending, T = torsion

## V. Conclusions

In this paper, the experimental identification of the modal parameters of the SHARCS system Smart Spring device has been carried out. In the operative conditions, the Smart Spring, installed at the nonrotating helicopter blade root, could adaptively vary the dynamic stiffness of the blade to change its elastic characteristics. The capability of the Smart Spring to change the dynamic behavior of the helicopter blade is demonstrated by analyzing the shifts in the modal parameters. The experimental investigations identified remarkable changes in the natural frequencies and damping ratios of the first and second torsional modes, whereas the flapwise bending modes are only marginally affected by the Smart Spring actuation. A beam finite element model has also been developed and a dynamic analysis conducted for an assessment of the model and for comparison of the modal properties with the experimental findings. This numerical model correlates well with the experimental results for lower-order bending and torsion modes, but it requires the use of different topology finite elements for the accurate prediction of both coupled and higher-order modes. This preliminary result needs further validation, both numerically and experimentally. Specifically, a numerical analysis aimed at evaluating the amount of vibration reduction and changes on the rotor vibratory loads is

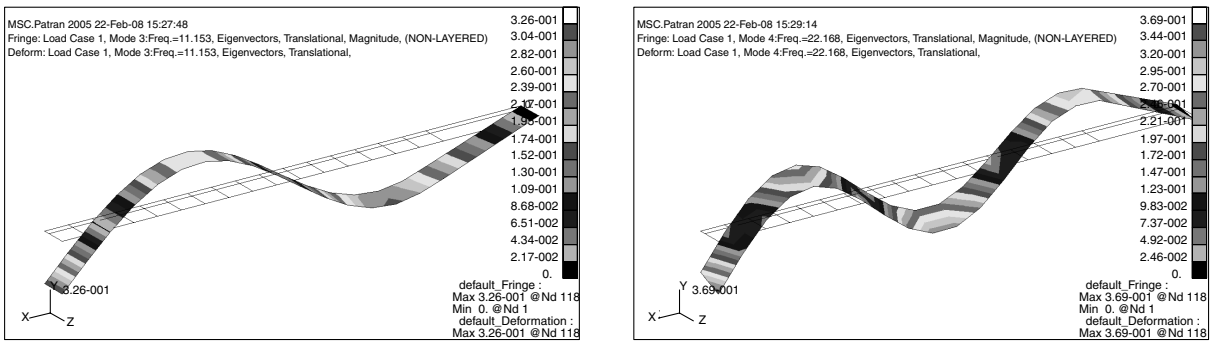


**a) FE Mode # 3 - $f_n$ =11.1535 Hz** **b) FE Mode # 4 - $f_n$ = 22.1684 Hz**

**Fig. 17 Mode shapes from FE analysis.**

needed. Moreover, future investigations will have to consider the actuators in working condition, that is, integrated in a control-loop system and with a rotating blade as test structure. Nevertheless, the results achieved in the experimental activity reported in this paper represent a milestone in the future developments of the Smart Spring system of the SHARCS project. These findings are the first experimental evidence of the capability of the Smart Spring to change the dynamic properties of a full-scale helicopter blade. Without these promising results, any other experimental and numerical developments would appear unjustifiable.

## Acknowledgments

This research has been partially supported by Progetto Giovani Ricercatori: Dinamica ed Aeroelasticità dei Rotori di Elicottero, University of Rome "La Sapienza," 2001. The authors wish to thank Chiara Valente for encouraging and supporting this activity.

## References

[1] Splettstoesser, W. R., Junker, B., Schulz, K. J., Wagner, W., Weitemeier, B., Protopsaltis, A., and Fertis, A., "The HELINOISE Aeroacoustic Rotor Test in the DNW: Test Documentation and Representative Results," DLR DLR-Mitt. 93-09, 1993.

[2] Jacklin, S. A., Blaas, A., Swanson, S. M., and Teves, D., "Second Test of a Helicopter Individual Blade Control System in the NASA AMES 40- by 80-Foot Wind Tunnel," *Proceedings of American Helicopter Society, 2nd International Aeromechanics Specialists' Conference*, American Helicopter Society, Alexandria, VA, 1995, pp. 7.9–7.26.

[3] Kube, R., van der Wall, B. G., Schultz, K.-J., and Splettstoesser, W. R., "IBC Effects on BVI Noise and Vibrations: A Combined Numerical and Experimental Investigation," *Proceedings of the 55th Annual Forum of the American Helicopter Society*, Vol. 2, American Helicopter Society, Alexandria, VA, May 1999, pp. 2282–2291.

[4] Arnold, U. T. P., and Fürst, D., "Closed Loop IBC Results from CH-53 G Flight Tests," *Aerospace Science and Technology*, Vol. 9, No. 5, July 2005, pp. 421–435. doi:10.1016/j.ast.2005.01.014

[5] Friedmann, P. P., Liu, L., and Patt, D., "Simultaneous Vibration and Noise Reduction in Rotorcraft Using Aeroelastic Simulation," *Journal of the American Helicopter Society*, Vol. 51, No. 2, Apr. 2006, pp. 127–140.

[6] Nitzsche, F., Grewal, A., and Zimcik, D. G., 1999, "Structural Component Having Means for Actively Varying its Stiffness to Control Vibrations," U.S. Patent No. 5,973,440. European Patent No. EP-996570-B1, 2001.

[7] Nitzsche, F., Zimcik, D., Wickramasinghe, V., and Yong, C., "Control Laws for an Active Tunable Vibration Absorber Designed for Aeroelastic Damping Augmentation," *The Aeronautical Journal*, Vol. 108, No. 1079, 2004, pp. 35–42.

[8] Feszty, D., Gillies, E. A., and Vezza, M., "Alleviation of Rotor Blade Dynamic Stall via Trailing-Edge-Flap Flow Control," *AIAA Journal*, Vol. 42, No. 1, 2004, pp. 17–25. doi:10.2514/1.853

[9] Aoyama, T., Kondo, N., Aoki, M., Nakamura, H., and Saito, S., "Calculation of Rotor Blade-Vortex Interaction Noise Using Parallel Super Computer," *22nd European Rotorcraft Forum, The Royal Aeronautical Society*, Vol. 2, Paper No. 81, 1996.

[10] Cesnik, C. E. S., and Shin, S.-J., "On the Modeling of Active Helicopter Blades," *International Journal of Solids and Structures*, Vol. 38, Nos. 10–13, March 2001, pp. 1765–1789. doi:10.1016/S0020-7683(00)00135-9

[11] Koratkar, N. A., and Chopra, I., "Wind Tunnel Testing of a Smart Rotor Model with Trailing-Edge Flaps," *Journal of the American Helicopter Society*, Vol. 47, No. 4, Oct. 2002, pp. 263–272.

[12] Coppotelli, G., Marzocca, P., Ulker, F. D., Campbell, J., and Nitzsche, F.,"SHARCS Project: Modal Parameters Identification of Smart Spring/Helicopter Blade System," *47 AIAA/ASME/ASCE/AHS/ASC, Structures, Structural Dynamics, and Materials Conference,* AIAA Paper 2006-2035, May 2006.

[13] Guillaume, P., Verboven, P., Vanlandiut, S., Van Der Auweraer, H., and Peeters, B., "Poly-Reference Implementation of the Least-Squares Complex Frequency-Domain Estimator," *Proceedings of IMAC 21, the International Modal Analysis Conference*, Society for Experimental Mechanics Paper No. 183, 2003.

[14] Verboven, P., "Frequency Domain System Identification for Modal Analysis," Ph.D. Thesis, Vrije Univ., Brussels, 2002.

[15] Guillaume, P., Verboven, P., Vanlanduit, S., Van Der Auweraer, H., and Peeters, B., "A Poly-Reference Implementation of the Least-Squares Complex Frequency-Domain Estimator," *IMAC 21, the International Modal Analysis Conference* [CD-ROM], edited by Society for Experimental Mechanics, Feb. 2003.

[16] Balis Crema, L., Coppotelli, G., and La Scaleia, B., "Identification and Updating of AB204 Helicopter Blade, F. E. Model by Means of Static and Dynamic Tests," *45 AIAA/ASME/ASCE/AHS/ASC, Structures, Structural Dynamics, and Materials Conference*, AIAA Paper 2004-1946, 2004.